

Effect of pressure recovery vanes on the performance of a swirl tube, with emphasis on the flow pattern and separation efficiency

Alex C. Hoffmann, Weiming Peng

Department of Physics and Technology, University of Bergen,
Allegt 55, 5007 Bergen, Norway

and

Huub Dries, Michiel Regelink, Kee-Khoon Foo

Shell Global Solutions, Shell Amsterdam,
PO Box 38000, 1030 BN Amsterdam, The Netherlands

December 7, 2006

Abstract

The effect of pressure recovery, or rectifying, vanes on the performance of reverse-flow swirl tubes has been investigated both by calculation based on velocity measurements and by direct pressure measurements. The calculations show that about 50% of the pressure drop should be recoverable. This result is compared with literature and is discussed in some detail. The experimental results show that rectifying vanes can recover some of the dynamic pressure in the swirling motion. The deeper the vanes extend into the separation space, the more is recovered. Importantly, however, the separation efficiency is reduced, and a Stk-Eu plot shows that installation of the vanes, at least in the positions tested here, does not improve the overall performance. Visualization also shows that the presence of the rectifying vanes destabilized the vortex, causing the vortex end to occur in the tube separation section, an issue not yet addressed in the literature. It is shown that flowvisualizations and CFD simulations indicate a type “0” vortex breakdown in the gas outlet, and that this may explain some of the observed phenomena related to rectifying vanes.

Key words: reverse-flow cyclone, rectifying vanes, pressure recovery, dynamic pressure, swirl, vortex breakdown

1 Introduction

Centrifugal dedusters are very widely used, for instance in fluidized catalytic cracking (FCC) units in the oil industry. Meeting new, stringent emission

limits puts extra demands on deduster design.

This study concentrates on reverse-flow, cylindrical swirl tubes with swirl vanes as shown in Figure 1. The gas flow pattern is sketched in the figure, the particles are centrifuged to the wall, and exit through the dust exit. This type of deduster design is simple and compact, and may perform at least as well as traditional cylinder-on-cone cyclones with tangential inlet.¹

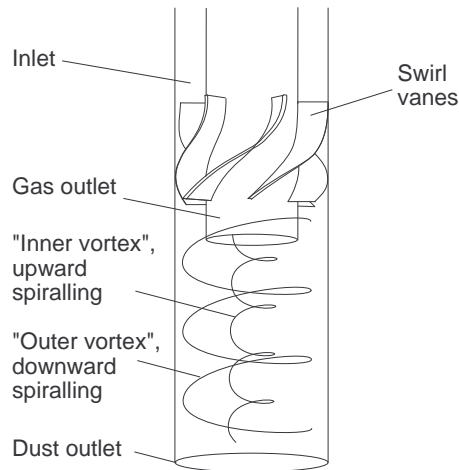


Figure 1: Sketch of a cylindrical swirl tube with swirl vanes, with the gas flow pattern indicated

The two performance indicators used for centrifugal separators are the pressure drop and the particle separation efficiency.

The gas exiting the gas outlet is swirling strongly, and the “dynamic pressure” in this motion is dissipated downstream without much recovery of static pressure. One idea has been to insert rectifying vanes in the gas outlet to recover static pressure. It is claimed^{2,3} that 30–50% of the pressure drop can be recovered in this way. However, little is published on the effect of rectifying vanes, specifically on the flow pattern and separation efficiency, in centrifugal separators.

At an early stage, Shepherd and Lapple³ reported rectifying vanes to reduce cyclone pressure drop by up to 50%, but also to reduce separation efficiency. Later works^{4,5} report that rectifying vanes, if placed downstream of the separator, can reduce pressure drop by 22% without reducing the separation efficiency. Muschelknautz and Brunner⁶ used a rectifier to reduce the pressure drop of cyclones by 15–20%.

The objective of this project is to analyse the effect of placing rectifying vanes in two different positions in the gas outlet of a reverse-flow centrifugal separator, and to measure and explain their effect both on the pressure drop and—crucially—the flow pattern and the separation efficiency.

2 Experiments

2.1 Test rig

The experimental set-up is shown in Figure 2.

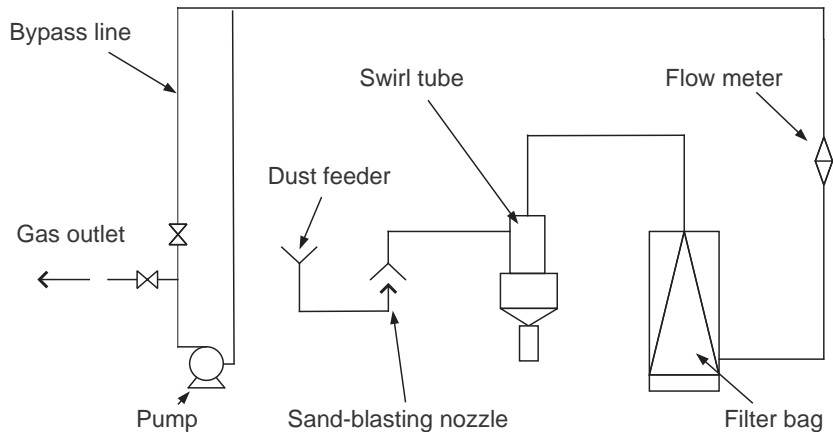


Figure 2: Sketch of the test rig for the performance tests

The gas flow is generated by a SAP-710 vacuum blower located downstream of the rig drawing the solids-laden gas through the system.

The gas is charged with test dust at the entrance of the system by a so-called sand-blasting nozzle, which breaks up agglomerates without the solids impacting on a solid surface. The test dust is fed to the sand blasting nozzle by a feeder, which transports the dust down to a container by using a motor-driven screw and a gas vibrator. The dust loading can be controlled by adjusting the motor speed.

Having passed the swirl tube, the gas flows through a Gore-tex membrane coated filter bag, which removes all the remaining dust particles. The filter bag can be weighed *in situ*.

The gas then flows through an “Annubar” flowmeter which operates by a similar principle to a Pitot tube, and has been calibrated by a Pitot tube and by the NMI (Nederlands Meet Instituut).

The swirl tube used in the experiments is a scaled (1:2) laboratory model of a Shell TSS swirl tube. The tube contains five swirl vanes with an exit angle to the horizontal of 30° . The laboratory model is made from Perspex, and a diagram is shown in Figure 3. A disadvantage of using Perspex is potential problems with static electricity. To avoid this the laboratory model was electrically grounded by wrapping it in conducting wire, which was connected to the metal frame of the rig.

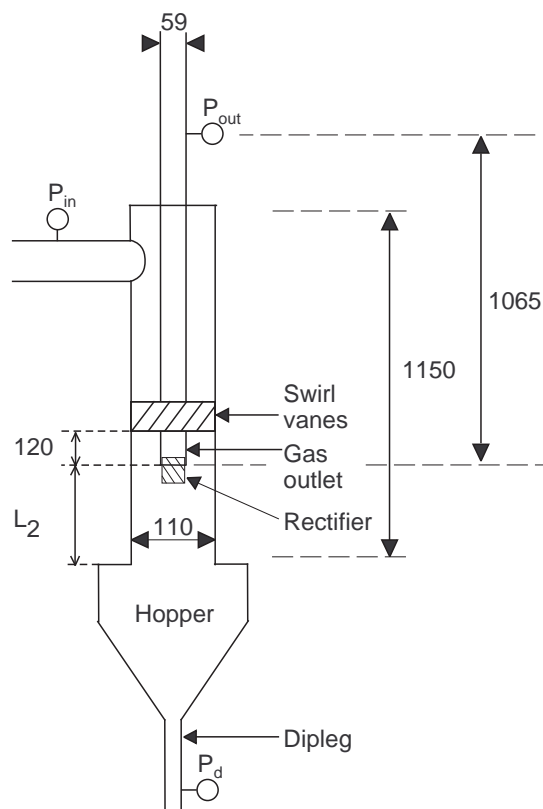


Figure 3: Sketch of the swirl tube, dimensions are in mm.

Rectifying vanes, sketched in Figure 4A were mounted in the gas outlet in two positions, called “high” and “low”, indicated in the Figure 4B. The vane assembly has an axial length of 73 mm and the three blades have an inlet angle of 70° to the horizontal.

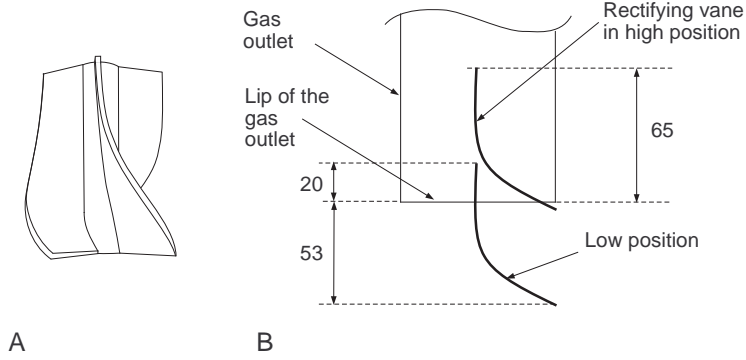


Figure 4: A: 3-D sketch of the rectifying vane assembly used. B: sketch showing the vane positions in the gas outlet

2.2 Measurements

The following static pressures can be measured around the swirl tube and flow meter:

1. P_{in} - the gauge pressure at the wall of the cyclone inlet
2. P_{out} - the gauge pressure at the wall of the gas outlet
3. P_d - the gauge pressure at the wall of the dipleg.

Two high-time-resolution pressure sensors PTX 120/WL from Druck Nederland bv, with an accuracy of 0.1%, were used.

Furthermore the pressures necessary to determine the flowrate by the Annubar flowmeter were monitored. Average values for the duration of the experiment are reported here.

In the efficiency tests, dust wall deposits were first allowed to equilibrate during a long pre-run at experimental conditions. Dust hopper and filter bag were then tared, the run carried out, and the hopper and filter bag weighed.

The overall fractional efficiency, η , is equal to:

$$\eta = \frac{m_c}{m_c + m_e} \quad (1)$$

where m_e and m_c are the masses of the lost and collected dust fractions, respectively.

The average dust load is calculated as mass of dust per unit volume of air from the known total mass of dust volume of air injected during the test.

2.3 Experimental conditions and materials

The experimental conditions were:

- Solids loading: 3 g/m³.
- Volumetric gas flow: from 150 to 300 m³/hr, corresponding to a mean axial gas velocity in the separation space between 4.4 and 8.8 m/s.

The test dust used was a fine fraction of a porous silica FCC catalyst base with a skeleton particle density of 2730 kg/m³ and an envelope density (*i.e.* including the internal pores) of 1500 kg/m³. The size distribution of the powder is shown in Figure 5.

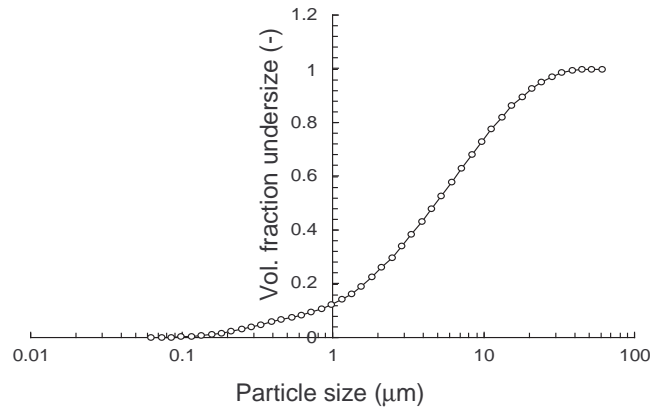


Figure 5: Size distribution of the fine FCC powder

3 Estimating the recoverable pressure

Below we calculate the pressure recovered by an ideal rectifier on basis of a mechanical energy balance over a control volume enclosing the rectifier as sketched in Figure 6. The analysis is non-standard in that the mechanical energy stored in flow tangential to the inflow surface is significant.

The total integrated mechanical energy balance over a control volume, which is possibly moving, $V(t)$ with surface $S(t)$ and containing the rectifier is:⁷

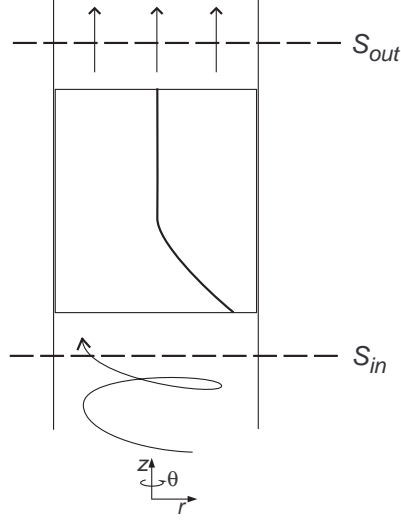


Figure 6: Sketch of the vane assembly showing the in- and outflow surfaces and the coordinate system

$$\begin{aligned}
& \int_{V(t)} \frac{\partial}{\partial t} \left(\frac{1}{2} \rho v^2 + \rho \hat{\Phi} \right) dV = - \int_{V(t)} \nabla \cdot \left(\frac{1}{2} \rho v^2 + \rho \hat{\Phi} \right) \mathbf{v} dV \\
& - \int_{V(t)} \nabla \cdot p \mathbf{v} dV - \int_{V(t)} \nabla \cdot (\boldsymbol{\tau} \cdot \mathbf{v}) dV + \int_{V(t)} p (\nabla \cdot \mathbf{v}) dV + \int_{V(t)} \boldsymbol{\tau} : \nabla \mathbf{v} dV,
\end{aligned} \tag{2}$$

where \mathbf{v} is the velocity vector with magnitude v ; ρ is the gas density, $\boldsymbol{\tau}$ is the deviatoric stress tensor, p is the pressure, and $\hat{\Phi}$ is the potential energy.

Applying Leibnitz' theorem to the left-hand-side and Gauss' divergence theorem to the first three terms on the right-hand-side gives:

$$\begin{aligned}
& \int_{V(t)} \frac{\partial}{\partial t} \left(\frac{1}{2} \rho v^2 + \rho \hat{\Phi} \right) dV = - \int_{S(t)} \mathbf{n} \cdot \left(\frac{1}{2} \rho v^2 + \rho \hat{\Phi} \right) (\mathbf{v} - \mathbf{v}_S) dS \\
& - \int_{S(t)} \mathbf{n} \cdot p \mathbf{v} dS - \int_{S(t)} \mathbf{n} \cdot (\boldsymbol{\tau} \cdot \mathbf{v}) dS + \int_{V(t)} p (\nabla \cdot \mathbf{v}) dV + \int_{V(t)} \boldsymbol{\tau} : \nabla \mathbf{v} dV,
\end{aligned} \tag{3}$$

where \mathbf{n} is the unit vector normal to the surface of the control volume and \mathbf{v}_S is the velocity of any moving surface in the control volume.

We assume that the flow is steady to make the left-hand-side zero. There are no moving surfaces, so that \mathbf{v}_S is zero, and V is not moving, so that S

and V are not functions of time. We neglect, as is normal, the work done by viscous forces at the in-and outflow surfaces, represented by the third term on the right-hand-side and we assume that the fluid is incompressible to make the fourth term on the right-hand-side zero. We also neglect flows of the potential energy $\hat{\Phi}$.

The balance then becomes:

$$0 = - \int_S \mathbf{n} \cdot \frac{1}{2} \rho v^2 \mathbf{v} dS - \int_S \mathbf{n} \cdot p \mathbf{v} dS + \int_V \boldsymbol{\tau} : \nabla \mathbf{v} dV, \quad (4)$$

where the last term is the integral of the dissipation function. If we consider a balance over an ideal rectifier, we neglect this term, and write:

$$0 = - \int_S \mathbf{n} \cdot \frac{1}{2} \rho v^2 \mathbf{v} dS - \int_S \mathbf{n} \cdot p \mathbf{v} dS \quad (5)$$

We use a cylindrical coordinate system (r, θ, z) and take the flow to be axisymmetrical, so that at a given z , v_z and v_θ are functions of r only. We further neglect the weak radial velocity component v_r , so that $v^2 = v_z^2 + v_\theta^2$.

We are interested in a balance over a horizontal surface, so that $\mathbf{n} \cdot \mathbf{v} = v_z$.

We split the surface integrals into contributions from the in- and outflow surface, S_{in} and S_{out} . Thus we obtain:

$$0 = -\frac{1}{2} \rho \int_{S_{in}} (v_z^2 + v_\theta^2) v_z dS + \frac{1}{2} \rho \int_{S_{out}} (v_z^2 + v_\theta^2) v_z dS - \int_{S_{in}} v_z p dS + \int_{S_{out}} v_z p dS \quad (6)$$

Assume that v_z and p are constant over S_{out} , equal to $v_{z,out}$ and p_{out} , respectively, and that v_θ is zero over S_{out} , then $\int_{S_{out}} v_z p dS = v_{z,out} p_{out} S_{out} = p_{out} Q$, where Q is the volumetric flowrate, and $\frac{1}{2} \rho \int_{S_{out}} (v_z^2 + v_\theta^2) v_z dS = \frac{1}{2} \rho v_{z,out}^3 S_{out} = \frac{1}{2} \rho v_{z,out}^2 Q$. Furthermore, the term $\int_{S_{in}} v_z p dS$ is, if divided by Q , the *mean static pressure in the fluid flowing through S_{in}* . We thus obtain:

$$\int_{S_{in}} v_z p dS - p_{out} Q = -\frac{1}{2} \rho \int_{S_{in}} (v_z^2 + v_\theta^2) v_z dS + \frac{1}{2} \rho v_{z,out}^2 Q \quad (7)$$

and dividing by Q :

$$\frac{\int_{S_{in}} v_z p dS}{Q} - p_{out} = \Delta p = -\frac{\rho}{2Q} \int_{S_{in}} (v_z^2 + v_\theta^2) v_z dS + \frac{\rho v_{z,out}^2}{2} \quad (8)$$

To find Δp we therefore require $v_z(r)$ and $v_\theta(r)$. To find them we appeal to experiment. Figures 7 and 8 show the tangential and axial gas velocity profiles just under the gas outlet in a conventional tangential inlet cyclone, and a swirl tube, respectively, measured by Laser Doppler Anemometry.⁸

We can calculate the total pressure recoverable by placing a rectifier just under the lip of the gas outlet by performing the integration in Eq. (8) over the gas entering the gas outlet. Call the gas outlet radius R_e . It turns out that the radial position of zero axial flow in both separators almost exactly coincide with R_e . We thus obtain:

$$\Delta p = -\frac{\rho}{2Q} \int_0^{R_e} (v_z^2 + v_\theta^2) v_z 2\pi r dr + \frac{\rho v_{z,out}^2}{2} \quad (9)$$

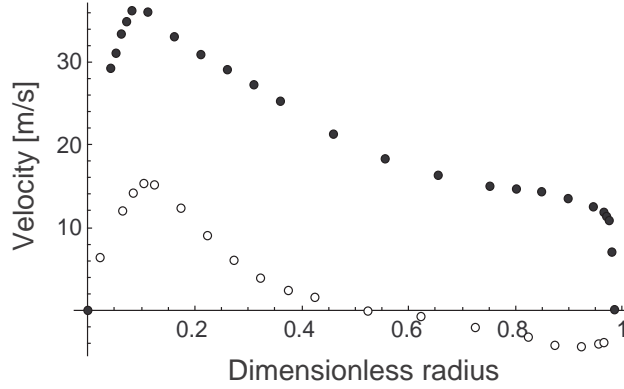


Figure 7: Tangential (filled circles) and axial (open circles) gas velocity just under the gas outlet in a cylinder-on-cone, tangential inlet cyclone

To perform the integration in Eq. (9), we need to fit functional forms to these velocity profiles. For the tangential velocity, it has been reported⁹ that the tangential velocity profile of Burger's vortex can be fitted well to the tangential velocity distribution in a cyclone:

$$\begin{aligned} v_z &= 2\sigma z, \\ v_r &= -\sigma r, \\ v_\theta &= \frac{\Gamma}{2\pi r} \left[1 - \exp\left(-\frac{r^2}{2\delta^2}\right) \right], \end{aligned} \quad (10)$$

where Γ is the total circulation.

When we tried to fit this it turned out, however, that Burger's vortex could not reflect the combination of narrow core and flat outer v_θ profile

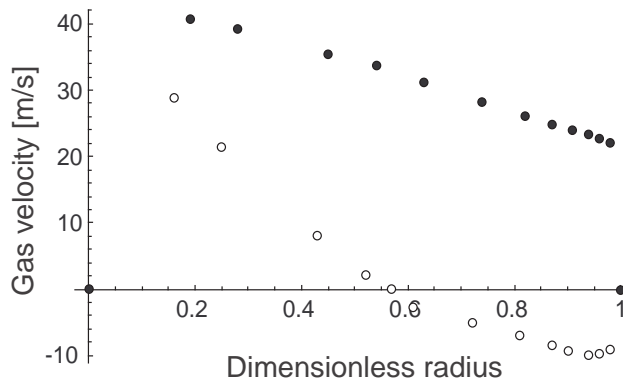


Figure 8: Tangential (filled circles) and axial (open circles) gas velocity just under the gas outlet in a cylindrical swirl tube with swirl vanes

shown in Figures 7 and 8 sufficiently well. For the axial velocity profiles, we do not have a known functional form available at all. We therefore fit both velocity profiles with simple interpolation functions.

Doing this and performing the integration numerically gave the results shown in Table 1. Also shown in this table are the total pressure drops measured over the two separators at these flowrates. Note that the outlet pressures are only approximations, since there would still have been some swirl present at the measurement points.

Table 1: Recoverable pressure by mounting rectifier at or below the lip of the gas outlet

	Recoverable pressure Eq. (9) [Pa]	Measured Δp [Pa]	% recoverable
Cyclone	411	800	51.3
Swirl tube	853	2100	40.6

Thus about half of the pressure drop should be recoverable in this way. We discuss the ramifications of this result further below.

4 Results and discussion

4.1 Pressure drop and flowpattern around the gas outlet

The tests were executed under a series of gas flows in the approximate range 140–300 m³/hr. The experimentally measured pressure drops gas inlet to the gas outlet, ($P_{out} - P_{in}$), and gas inlet to dipleg ($P_d - P_{in}$) are shown in the Figures 7 and 8, respectively. We note already here that the measurements

of P_{out} and P_d are complicated by any swirl present at these positions. In this configuration, the P_{out} pressure point was quite far downstream from the separator, as shown in Fig. 3, and we do not expect that the error in the measured pressure drop caused by the presence of swirl there is very large.

We see that the measured overall pressure drop ($P_{out} - P_{in}$) is the highest without the pressure recovery vanes, with the exception of the highest flowrate $Q = 300 \text{ m}^3/\text{s}$, the “no vane” case representing a special case in terms of the flow in the tube, as we will discuss below.

In general the overall pressure drop decreases with the installation of the rectifier or pressure recovery vane, and the longer the vane extends into the separation space, the lower is the measured overall pressure drop, indicating that more dynamic pressure is recovered with the vane in the lower position than in the high position.

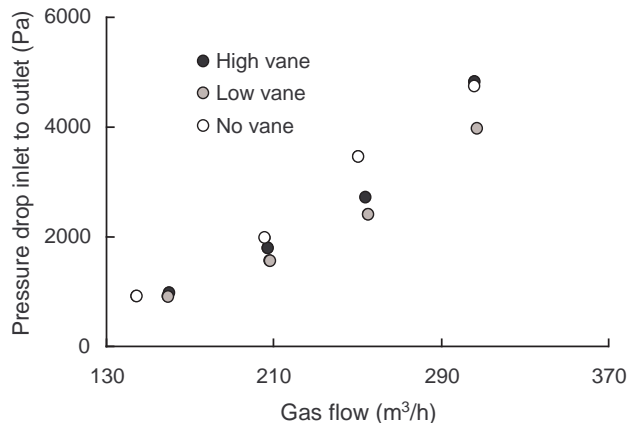


Figure 9: Measured pressure drop inlet to gas outlet

We noted above that the presence of swirl at a pressure tapping will make the static pressure at the wall higher than the cross-sectional average, and the average in the flowing gas. Figure 3 shows that the pressure point for p_{out} was a meter downstream of the mouth of the gas outlet, so that the swirl, and therefore its effect on the radial static pressure distribution is not very strong, but it is likely to make the recovered pressure drop appear lower than it actually is. The maximum reduction in measured pressure drop in Figures 9 are 30.4% and 21% for the low and high rectifier positions, respectively, both achieved at a gas flow of $255 \text{ m}^3/\text{hr}$.

We mentioned in the introduction that rectifying vanes have been reported³ to reduce cyclone pressure drop by as much as 50%, but to reduce the separation efficiency, but also that they, if they are placed higher in the gas outlet,^{4,5} reduce pressure drop much less, around 22% but without reducing the separation efficiency.

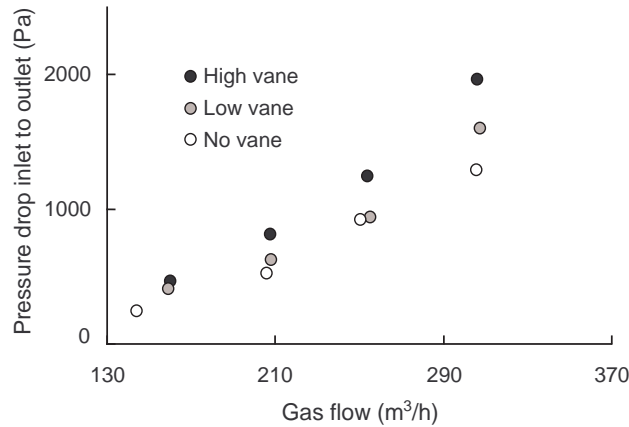


Figure 10: Measured pressure drop inlet to dipleg

A possible explanation for this may be the existence of an axisymmetric (type “0” according to Faler and Leibovich¹⁰) vortex breakdown in the gas outlet.

Figure 11 shows the flowpattern in the gas outlet and downstream tubing of a similar swirl tube as the present one (but with a tapered gas outlet, the present one is cylindrical) visualized with helium bubbles.¹¹ The streaklines of the neutral buoyancy tracer are clearly diverging in the gas outlet, consistent with a type “0” vortex breakdown. The clear formation of a core in the downstream tubing shows that there was still some vortex motion present there.

We also note that the numerical simulations of Derksen¹² in a swirl-tube-like geometry shows type “0” vortex breakdown in the cylindrical gas outlet, see figure 12.

Such a breakdown close to the mouth of the gas outlet would reduce the swirl dramatically, and explain that a much higher pressure drop recovery is possible if the rectifier is placed protruding into the separation space itself rather than higher in the gas outlet, downstream of such a vortex breakdown. It would also explain why placing it in the former position rather than downstream of a breakdown would disturb the flow in the separation space so much more.

The existence of such a breakdown is also consistent with the traditional notion that most of the cyclone pressure drop, some say as much as 80–90%, is incurred in—or associated with—the gas outlet. It is likely that some of the dissipation due to the presence of the gas outlet extends into the separation space. Figure 11 shows the vortex core being disturbed in the separation space under the gas outlet.

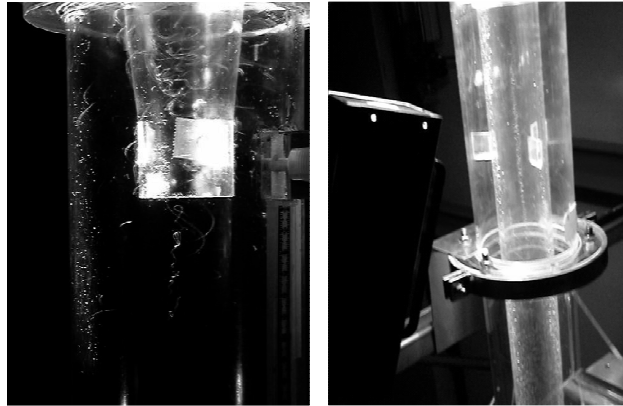


Figure 11: Visualization of the flow in the gas outlet and downstream tubing in a swirl tube

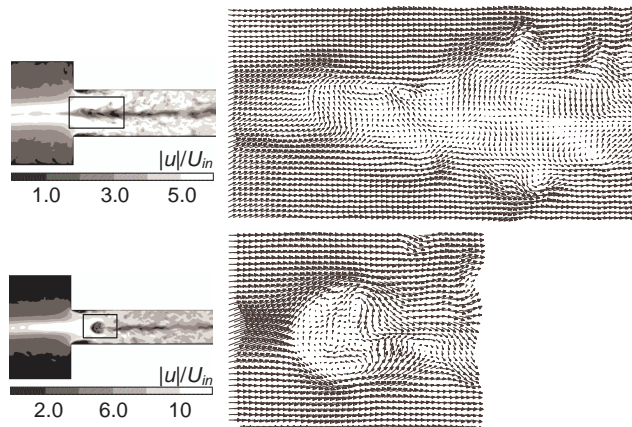


Figure 12: CFD simulations of Derksen showing type “0” vortex breakdown in the gas outlet of a swirl-tube-like geometry, reprinted from,¹² copyright 2004, with permission from Elsevier

4.2 Separation efficiency and flowpattern in the separation space

The experimental results for the overall separation efficiency are shown in Figure 13. The unbiased estimate for standard deviation due to experimental error based on six repeat experiments was 0.37%.

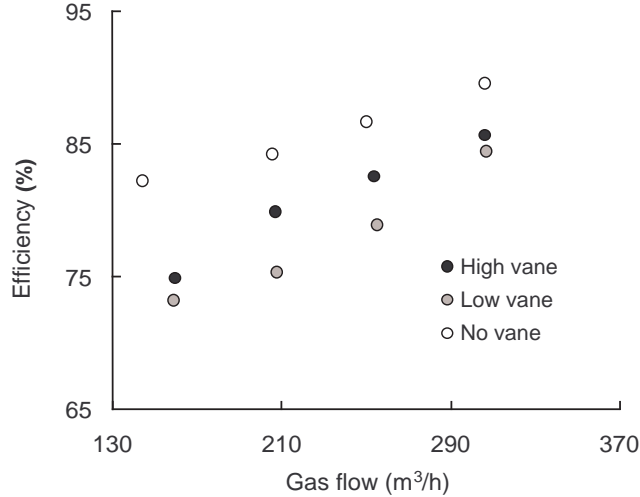


Figure 13: The separation efficiency

The results clearly show that the presence and the position of the rectifying vanes has a significant influence on the separation efficiency of the swirl tube: installation of the rectifier leads to a lower efficiency, and the lowest efficiency is seen with the rectifier in the low position.

We can convert the over-all efficiencies to approximate cut-sizes for the swirl tube in the following way:

If we know the cumulative volumetric size distribution of the feed:

$$F(d_p) = \int_0^{d_p} f(x)d(x) \quad (11)$$

and we assume that all material below the cut size d_{p50} is lost and all above is collected, we can calculate d_{p50} from:

$$F(d_{p50}) = 1 - \eta_{overall}. \quad (12)$$

The results of calculating the cut sizes are shown in Figure 14.

To lend credence to these results it is preferable to compare with the predictions of some proven model for cyclone separation performance. In Figure 14 the predictions of the classical model of Barth¹³ and an empirical

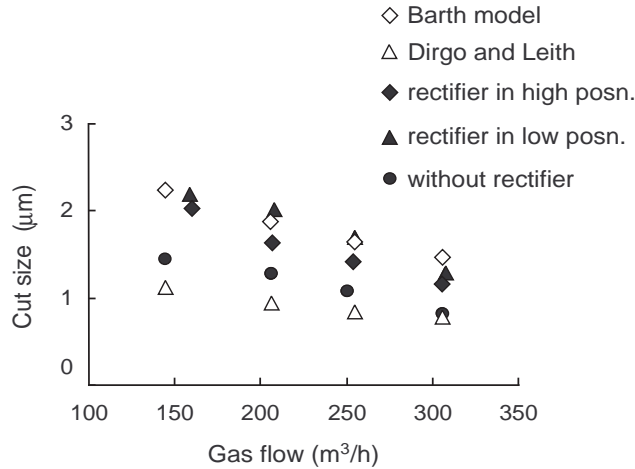


Figure 14: Cut sizes calculated from the size distribution of the feed, given in Figure 5, and Equation (12) together with the predictions of the classical cyclone model of Barth and the empirical correction of Dirgo and Leith, both adapted to swirl tubes

correction of it by Dirgo and Leith,¹⁴ both adapted to swirl tubes by the method of Peng et al.,¹ are also shown. The model predictions are seen to agree quite well with the results in terms of the trend. Also the results all fall between the two model predictions. The model of Barth is known often to err on the conservative side, a fact that prompted the empirical correction of Dirgo and Leith.

In addition to decreasing the separation efficiency, probably due to decreasing the swirl velocity in the separation space, the presence of the pressure recovery vanes was also seen to destabilize the vortex. In earlier work¹⁵ we have studied the “end of the vortex” phenomenon and the effect of the length of the vortex on the pressure drop. We found that the separation efficiency improves and the pressure drop decreases if the vortex is long. In this work, we found that the end of the vortex could be observed in the swirl tube under all experimental conditions, except at the highest flowrate without the rectifier and without dust injection, where the core would centralize, and the vortex extend all the way down to the bottom of the hopper. A result of this was the somewhat low inlet to outlet pressure drop at 300 m³/s seen in Figure 9. A centralized vortex core could not be achieved with any gas flowrate with the rectifier installed, the end of the vortex was always in the tube, as also evidenced by the wall deposits in the tube under the position of the vortex end (Figure 15).

Earlier work showed that wall roughness has the effect of destabilizing the vortex, causing the vortex end to appear in the tube and this work shows

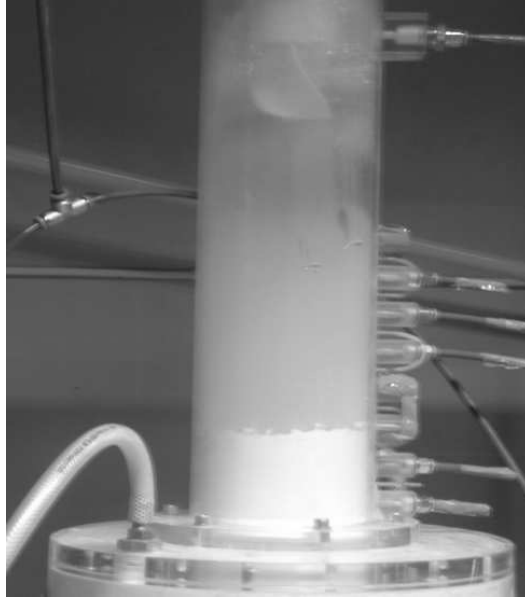


Figure 15: Wall deposits after an experiment showing the end of the vortex to have been positioned in the swirl tube

the rectifier to have the same effect.

4.3 The over-all performance of the swirl tube

Svarovsky¹⁶ gives the following expression for the performance of gas cyclones:

$$\text{Eu}\sqrt{\text{Stk}_{50}} = \sqrt{12} \quad (13)$$

with:

$$\text{Eu} \equiv \frac{\Delta P}{\frac{1}{2}\rho v_a^2} \quad \text{and} \quad \text{Stk}_{50} \equiv \frac{(\rho_p - \rho_g) d_{p50}^2 v_a}{18\mu_g D}.$$

Here v_a is the cross-sectional mean axial gas velocity in the tube body, μ_g is the gas viscosity and ρ_p the particle density. The experimental results are shown in a plot of $\ln(\text{Eu})$ vs. $\ln(\text{Stk}_{50})$ in Figure 16.

In contrast to earlier work, we are not attaching significance to the absolute position of the points here. In this work, values of Stk are based on a size distribution measured by laser diffraction, which is moreover general for this class of powder, while in earlier work, we based Stk on size distributions measured for the specific powder sample by centrifugation techniques. We therefore leave the axis scales out of the figure, and simply compare the points for the different configurations with a line of the form $\text{Eu}\sqrt{\text{Stk}_{50}} = C$, where C is a constant fitted so that the line runs through the points generated with the configuration without rectifier. This type of plot shows us the relative performances of the different configurations.

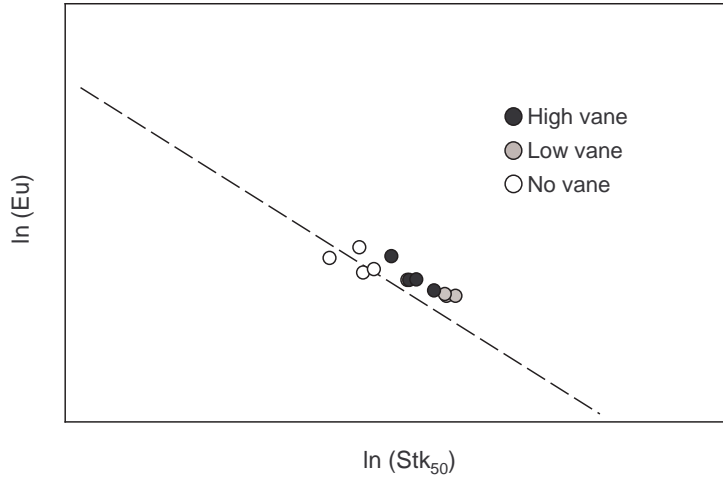


Figure 16: $\ln(\text{Eu})$ plotted against $\ln(\text{Stk}_{50})$ for the swirl tube with and without rectifier compared with a line of the form $\text{Eu}\sqrt{\text{Stk}_{50}} = C$. The axis scales have been left out due to the factors mentioned in the text

Studying the figure, it is not clear that including the rectifier has a positive influence on the over-all performance, on the contrary, the points with the rectifier included lie above the line. It has to be kept in mind, however, that some swirl was still present at the measurement point without the rectifier installed, causing the pressure drop to appear lower than it actually is.

4.4 Experimental errors

To estimate the accuracy of the measured values, one particular experiment was executed 6 times, namely that with the rectifier in the low position and a gas flow of $Q = 250 \text{ m}^3/\text{h}$. The unbiased estimate of the standard deviation of the individual results, x_i due to experimental error was determined, and from that the 95% confidence interval as:

$$\text{CONF } 95\% = \sqrt{\frac{\sum(x_i - \langle x \rangle)^2}{n-1}} 1.96 \quad (14)$$

The 95% confidence interval for the mean of the six experimental values was found by dividing by $\sqrt{6}$.

The 95% confidence intervals for the individual results are: 0.73%, 104 Pa and 47 Pa for the separation efficiency, the pressure drop inlet to outlet and the pressure drop inlet to dip leg, respectively, while the corresponding numbers for the means of the repeated experiments are: 0.30%, 42 Pa and 19 Pa, respectively.

5 Conclusions

The itemized conclusions are:

- A first-principles analysis has been given of the effect of a rectifier. This analysis is non-standard, since there is a significant amount of energy stored in motion oblique to the inlet surface of the control-volume.
- An estimate for the recoverable static pressure has been calculated *based on velocity measurements*, and the estimate has been shown to be credible by comparing with experimental data from the literature.
- A consistent set of experimental results showing the effect of rectifiers on the pressure drops inlet to outlet and inlet to dipleg have been given.
- It has been shown that installing rectifying vanes low in—or under—the gas outlet reduces the cyclone pressure drop by up to 30%, but also disturbs the flowpattern in the separation space causing the separation efficiency to decrease. It has also been shown to destabilize the vortex; so much so that a rectifier can cause the end of the vortex to appear in the swirl tube.
- The effect of rectifying vanes on cyclone separation efficiency has been quantified, and the overall effect on cyclone performance has been assessed using a Stokes-Euler plot.
- A plausible explanation has been given to the question of why the effect of rectifying vanes is so different, depending on whether they are mounted in the mouth of the gas outlet or further downstream. The explanation is based on the existence of a type “0” vortex breakdown in the gas outlet, which is supported by both experiments using neutrally boyant tracers and CFD simulations.

References

1. Peng, W.; Hoffmann, A. C.; Dries, H. W. A. *AIChE Journal* **2004**, *50*, 87–96.
2. Hoffmann, A. C.; Stein, L. E. *Gas Cyclones and Swirl Tubes—Principles, Design and Operation*; Springer Verlag: Berlin, 2002.
3. Shepherd, C. B.; Lapple, C. E. *Ind. & Eng. Chem.* **1940**, *32*, 1246–1248.
4. Browne, J. M.; Strauss, W. *Atmospheric Environment* **1978**, *12*, 1213–1221.
5. Olszewski, A.; Strauss, W. *Atmospheric Environment* **1978**, *12*, 1559–1559.
6. Muschelknautz, E.; Brunner, K. *Chem. Ing. Techn.* **1967**, *39*, 531–538.
7. Bird, R. B.; Stewart, W. E.; Lightfoot, E. N. *Transport phenomena*; John Wiley and Sons: New York, 2. ed.; 2002.
8. Peng, W.; Hoffmann, A. C.; Boot, P.; Udding, A.; Dries, H. W. A.; Ekker, A.; Kater, J. *Powder Technol.* **2002**, *127*, 212–222.
9. Marcu, B.; Meiburg, E.; Newton, P. K. *Phys. Fluids* **1995**, *7*, 400–410.
10. Faler, J. H.; Leibovich, S. *Physics of Fluids* **1977**, *20*, 1385–1400.
11. Peng, W.; Hoffmann, A. C.; Dries, H. W. A.; Regelink, M.; Foo, K.-K. *Meas. Sci. Technol.* **2005**, *16*, 2405–2414.
12. Derksen, J. J. *Computers & Fluids* **2005**, *34*, 301–318.
13. Barth, W. *Brennstoff-Wärme-Kraft* **1956**, *8*, Heft 1, 1–9.
14. Dirgo, J.; Leith, D. *Filtration and Separation* **1985**, *22*, 119–125.
15. Peng, W.; Hoffmann, A. C.; Dries, H. W. A.; Regelink, M. A.; Stein, L. E. *Chem. Eng. Sci.* **2005**, *60*, 6919–6928.
16. Svarovsky, L. Solid-Gas Separation. In *Gas Fluidization Technology*; Geldart, D., Ed.; Wiley: New York, 1986.